



REGULAR ARTICLE

Determination of Areas on the Surface of Optical Fairings of Various Geometric Shapes Subjected to Maximum Thermal Shock Impacts

I.V. Yatsenko^{1,*} , V.S. Antonyuk², V.A. Vashchenko¹, V.I. Gordienko¹, S.O. Kolinko¹, T.I. Butenko¹

¹ Cherkasy State Technological University, 18006 Cherkasy, Ukraine

² National Technical University of Ukraine "Kyiv Polytechnic Institute named after Igor Sikorsky", 03056 Kyiv, Ukraine

(Received 01 November 2024; revised manuscript received 20 February 2025; published online 27 February 2025)

Mathematical models have been developed to describe the heating of optical fairings of infrared (IR) devices with various geometric shapes (hemispherical, pyramidal, etc.) under the influence of an external supersonic airflow. Areas on the surface of the fairings subjected to maximum thermal shock impacts have been identified for different flow regimes (laminar, turbulent), which lead to their destruction and IR device failures during firing and flight conditions. The advantages and disadvantages of the considered fairing geometries have been established depending on their flight speed. It has been established that, for the specified ranges of flight velocities, as in the case of hemispherical fairings, a turbulent flow regime is realized over most of their surfaces, and hazardous areas emerge. By additionally treating these areas with an electron beam (which increases the resistance of surface layers to thermal and mechanical impacts), their destruction during operation can be prevented. In this case, the intensity of the pressure gradient's impact on the fairing is reduced. Therefore, during the operation of fairings with different geometric shapes at high flight speeds (above $2 \cdot 10^3 \dots 3 \cdot 10^3$ m/s), the thermal and mechanical impact (due to pressure gradients in the shock wave) is more intense for fairings with sharp leading edges (pyramids, cones, etc.), leading to their faster destruction under flight conditions.

Keywords: Optoelectronic instrumentation, Optical elements, Mathematical models, Supersonic airflow, Infrared (IR) devices in shot and flight conditions, Optical ceramic, Electron-beam technology

DOI: [10.21272/jnep.17\(1\).01030](https://doi.org/10.21272/jnep.17(1).01030)

PACS number: 42.79.Bh

1. INTRODUCTION

The continuously increasing demands for the application of infrared (IR) devices with optical fairings of various geometric shapes (hemispherical, pyramidal, etc.) for self-guidance and observation of different objects (with firing velocities exceeding $2 \cdot 10^3$ m/s and angular velocities of axisymmetric rotation exceeding $4 \cdot 10^3$ rad/s) have led to significant operational instabilities, anomalies, and failures. The primary cause of these issues is the uneven surface heating of optical ceramic fairings (e.g., KO1, KO2) under conditions of supersonic airflow, resulting in substantial thermoelastic stresses. These stresses occur on surface areas subjected to maximum external thermal shock impacts that exceed the critical thresholds of the specific ceramic materials. This leads to cracking, chipping, and, ultimately, the destruction of the fairings. Experimental studies of IR devices [1-6] have shown that the location of these critical areas on the surface of fairings, as well as the nature of their destruction, significantly depends on the geometric shape of the fairing and the airflow regime (laminar or turbulent). Therefore, to enhance the reliability of IR devices during firing and flight, it is necessary to predict,

at the design stage, the areas on the fairing surface that are exposed to maximum external thermal shock impacts under various airflow regimes and exposure times. These critical areas can be further thermally strengthened during the final processing of the fairings, for example, using electron-beam technology, which is widely applied in optical instrumentation [5-8, 11, 12, 17].

To date, the above-mentioned issues have not been sufficiently studied. Specifically, the processes of heating optical ceramic fairings (e.g., KO1, KO2) in the form of hemispherical shells under counter-flow supersonic air streams over a wide range of velocities (exceeding $2 \dots 3 \cdot 10^3$ m/s) remain unexplored. Furthermore, the influence of the geometric shape of the fairing on its heating processes under conditions of supersonic airflow and the identification of areas subjected to maximum external thermal shock impacts have not been adequately investigated.

Therefore, the aim of this study is to develop a mathematical model of the heating process of fairings under a supersonic gas flow and to determine the influence of their geometric shape on the location of areas subjected to maximum external thermal shock impacts on the fairing surface under different flow regimes.

* Correspondence e-mail: i.yatsenko@chdtu.edu.ua



2. THE RESULTS OF THE RESEARCH AND THEIR ANALYSIS

Currently, in the study of heat transfer in solid bodies at the gas-solid boundary, third-kind boundary conditions (Newton's law) are typically applied, which incorporate the heat flux q_w [9-11]. This approach attempts to describe the complexity of heat exchange processes in the boundary layer and the solid body through the introduction of a single coefficient q_w . This coefficient is determined using empirical or semi-empirical formulas derived from experimental data obtained during aerodynamic tunnel tests of the objects [12-14]. However, such a formulation does not account for the mutual thermal influence between the solid body and the gas. Evidently, this approach to external heat exchange problems is not physically rigorous and thus requires specific justification for each particular case.

This way, in studies [10, 14, 15], it was shown that for highly conductive materials ($\lambda_T = 10...20$ W/m·K), with parameter values $\chi = 0.5^* (\lambda_c / \lambda_T)^* (\text{Re}_\infty)^{1/2} < 1$ (λ_T , λ_c being the thermal conductivity coefficients of the gas flow and the solid material, respectively; $\text{Re}_\infty = U_\infty \cdot l / \nu_T$, where U_∞ , ν_T are the velocity and kinematic viscosity of the gas flow, and l is the characteristic dimension of the body, such as the diameter of an axisymmetric object or the thickness of a flat body), the differences in temperature distributions on the body's surface obtained by solving the coupled problem and using the described method do not exceed 10-15%. Thus, strictly speaking, in this specific case, the use of Newton's law and the application of the standard Nusselt number formula ($NU = q_w \cdot l / \lambda_c (T_w - T_c)$, where T_w , T_c is the surface temperature of the body and recovery temperature in the boundary layer, representing the air temperature in the immediate vicinity of the body's surface) is justified [15, 16].

Thus, for values $1 < \chi < \infty$ (which typically correspond to poorly conductive materials under realistic incoming flow parameters), heat transfer calculations based on commonly used formulas that do not account for the thermophysical and geometric characteristics of the body – i.e., those that neglect the mutual thermal interaction between the body and the incoming flow – will result in significant errors (exceeding 10-15 %).

At the same time, for values $0 < \chi < 1$ (which typically correspond to highly conductive materials), commonly used formulas can be applied.

If, for example, to estimate the value of the parameter χ for optical ceramics KO1 ($\lambda_T = 15$ W/m·K), KO2 ($\lambda_T = 17$ W/m·K), KO3 ($\lambda_T = 17,5$ W/m·K), KO5 ($\lambda_T = 44$ W/m·K) and KO12 ($\lambda_T = 14,7$ W/m·K), then for the real parameters of the oncoming turbulent flow ($U_\infty = 10^3$ m/c; $\text{Re}_\infty = 10^6$; $\lambda_c = 2,04 \cdot 10^{-2}$ W/m·K), we obtain the following parameter values χ : for KO1 – $\chi \approx 0,66 < 1$; for KO2 – $\chi \approx 0,59 < 1$; for KO3 – $\chi \approx 0,57 < 1$; for KO5 – $\chi \approx 0,23 < 1$; for KO12 – $\chi \approx 0,68 < 1$.

Thus, for calculating the heat transfer between fairings made of the considered ceramics and an incoming supersonic turbulent flow, the specified method can be used with an error not exceeding 10-15%.

For laminar flow regimes ($\text{Re}_\infty < 10^5$), for all the

considered ceramics, the value $\chi \ll 1$, meaning that this method can indeed be applied in this case, but within the previously mentioned error margin. However, significantly more accurate results (with an error range of 5-10%) can be obtained by solving the problem of the body's airflow as a coupled problem.

Mathematical Modeling of the Thermal Impact of Supersonic Airflow on Hemispherical Fairings.

The gas-dynamic problem (Fig. 1) will be considered as quasi-steady, which is valid for most practical cases, except for impulsive regimes. This is due to the fact that the volumetric heat capacity of the gas flow (C_V) is small compared to the volumetric heat capacity of the fairing material (C_V), i.e., $(C_V / C_V) \ll 1$. Assuming that the gas flow is incompressible (which is valid for $u_\infty < 2 \cdot 10^3 \dots 3 \cdot 10^3$ m/s), the heat flux $q_n = \text{const}$ from the boundary layer (with zero attack and slip angles) is given by the following expression:

$$q_n = \frac{f(\text{Pr})}{\left(\frac{\rho_\delta \times u_\delta \times x}{\mu_\delta} \right)^{1/5}} \times \rho_\delta \times u_\delta \times C_p \times (T_r - T_w) \quad (1)$$

where $f(\text{Pr})$ – is a given function of the Prandtl number, which depends on the geometric shape of the body and the flow regime ($\text{Pr} = C_p^* \mu / \lambda_c$; ρ , u , μ , C_p , λ_c – respectively, density, speed along the x coordinate, dynamic coefficient viscosities, heat capacity and coefficient of thermal conductivity of the gas flow; T_w – fairing surface temperature; index “ δ ” – conditions on the outer boundary of the boundary layer [9, 18].

$$T_r = T_\delta \left(1 + 0,2 \cdot \bar{r} \cdot M^2 \right) \quad (2)$$

where \bar{r} – is the recovery coefficient, which characterizes the portion of the kinetic energy of the external air flow that transitions into heat capacity upon complete flow deceleration (for laminar flow, typically $\bar{r} = 0,85$, and for turbulent flow $\bar{r} = 0,88 \dots 0,90$); M is the Mach number ($M = u_\infty / u_*$, where u_* – is the speed of sound in air).

It is further assumed that for regions near the critical point, the equality $u_\infty = \bar{\beta} \cdot x$ holds, where $\bar{\beta}$ is a function of the u_∞ number for the undisturbed flow just before the shock wave (for laminar flow, this relationship was derived through pressure measurements and velocity calculations). Substituting equality $u_\infty = \bar{\beta} \cdot x$ into (1) gives:

$$q_n = f(\text{Pr}) \cdot \bar{\beta}^{4/5} \cdot \mu_\delta \cdot x^{3/5} \cdot C_p \cdot (T_r - T_w) \quad (3)$$

By substituting known gas-dynamic relationships [9, 18] into Eq. (3), we obtain the following expression for the heat flux in the case of turbulent flow:

$$q_n = \frac{0,00042}{\text{Pr}^{2/3}} \cdot \left(\frac{\bar{\beta} \cdot R_w}{u_\infty} \right)^{4/5} \cdot \left(\frac{u_\infty}{u_\infty \cdot x_0} \right)^{1/5} \cdot \left(\frac{\rho_\delta}{\rho_\infty} \right)^{4/5} \times \left(\frac{\mu_\delta}{\mu_\infty} \right)^{1/5} \cdot \rho_\infty \cdot u_\infty \cdot C_p \cdot (T_r - T_w) \cdot (\sin \theta)^{3/5} \quad (4)$$

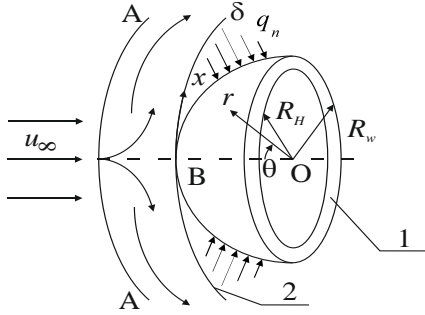


Fig. 1 – Schema of the heating of a hemispherical fairing: 1 – hemispherical shell made of optical material; B – frontal critical point (flow velocity equals zero); 2 – outer boundary of the boundary layer with thickness δ ; r , θ – spherical coordinates; R_w , R_H – radii of the outer and inner surfaces of the fairing, respectively; index “ ∞ ” – parameter values in the incoming air flow

Similarly, for the laminar flow regime over a hemisphere, the heat flux can be expressed as:

$$q_n = \frac{0,0083}{Pr^{2/3}} \cdot \left(\frac{\bar{\beta} \cdot R_w}{u_\infty} \right)^{1/2} \cdot \left(\frac{v_\infty}{u_\infty \cdot x_0} \right)^{1/2} \cdot \left(\frac{\rho_\delta}{\rho_\infty} \right)^{1/2} \times \left(\frac{\mu_\delta}{\mu_\infty} \right)^{1/2} \cdot \rho_\infty \cdot u_\infty \cdot C_p \cdot (T_r - T_w) \quad (5)$$

In formulas (4) and (5), the expression for $\bar{\beta}$ has the form:

$$\bar{\beta} = \frac{u_\infty}{2 \cdot R_w} \cdot \left(\frac{8 \cdot (\gamma_\infty - 1) \cdot M^2 + 2}{(\gamma_\infty + 1) \cdot M^2} \right) \times \left[1 + \frac{\gamma_\infty - 1}{2} \cdot \frac{(\gamma_\infty - 1) \cdot M^2 + 2}{2 \cdot \gamma_\infty \cdot M^2 - (\gamma_\infty - 1)} \right]^{\frac{1}{\gamma_\infty - 1}} \quad (6)$$

The relationships ρ_δ/ρ_∞ and μ_δ/μ_∞ are determined by calculating the pressure using Newton's method and the adiabatic expansion from the critical point along the fairing surface (in the direction of x).

$$\frac{\rho_\delta}{\rho_\infty} = 6,35 \cdot \left(1 - \frac{1}{7 \cdot M^2} \right)^{-2,5} \cdot \left(1 + \frac{5}{M^2} \right)^{-1} \cdot \bar{P}^{-5/2} \quad (7)$$

$$\frac{\mu_\delta}{\mu_\infty} = 0,447 \cdot M \cdot \left(1 + \frac{5}{M^2} \right)^{-1/2} \cdot \frac{1 + S/T_\infty}{1 + S/T_T} \cdot \bar{P}^{-3/14} \quad (8)$$

where S – is Sutherland's constant ($S = 110,4$ K); \bar{P} is the ratio of the pressure at the outer boundary of the boundary layer P_δ to the stagnation pressure P_T ; and T_T is the stagnation temperature. Based on the comparison of experimental data, a fairly accurate formula for determining the pressure distribution in the θ direction was obtained:

$$\bar{P} = 1 - (1,525 - 1,85 \cdot \bar{k}_0) \cdot (\sin \theta)^2 + (0,487 - 1,323 \cdot \bar{k}_0) \cdot (\sin \theta)^4 \quad (9)$$

where \bar{k}_0 – is the air compression factor across the normal shock wave:

$$\bar{k}_0 = \frac{\gamma_\infty - 1}{\gamma_\infty + 1} + \frac{2}{(\gamma_\infty + 1) \cdot M^2} \quad (10)$$

The stagnation pressure at the critical point is determined using the formula:

$$P_T = P_\infty \cdot M^2 \cdot \frac{\gamma_\infty - 1}{2} \cdot \left[\frac{(\gamma_\infty - 1) \cdot M^2}{4 \cdot \gamma_\infty \cdot M^2 - 2 \cdot (\gamma_\infty - 1)} \right]^{\frac{1}{\gamma_\infty - 1}} \quad (11)$$

The braking temperature has the form:

$$T_T = T_\infty \cdot \left(1 + \frac{\gamma_\infty - 1}{2} \cdot M^2 \right) \quad (12)$$

In the calculations, the Pr s for air can be considered constant and equal to 0,71, as it has minimal dependence on temperature. Similarly, the specific heat capacity of air C_p for the case of ideal gas flow can also be assumed constant, with a value of $C_p = 10^3$ J/kg·K.

Using the derived formulas (4) and (5) and standard application software packages, calculations of heat flux distributions from the boundary layer q_n along the surface of the fairing were performed for various flight conditions of the objects (Figs. 2–5).

From the results of the calculations presented in Figs. 2–5, it follows that the locations of the maximum heat flux values $(q_n)_{\max}$ on the surface of the fairing significantly depend on the flow regime. For the laminar flow regime $(q_n)_{\max}$, the maximum heat flux values are located near the front critical point ($\theta = 0^\circ$) of the fairing. For the turbulent flow regime, the maximum heat flux values $(q_n)_{\max}$ shift from θ to θ_{\max} . As the airflow velocity increases from $u_\infty = 7 \cdot 10^2$ m/s to $u_\infty = 2 \cdot 10^3$ m/s, the heat flux values $(q_n)_{\max}$ increase from $0,3 \cdot 10^6$ W/m² to $2,3 \cdot 10^6$ W/m² for the turbulent flow regime and from $0,2 \cdot 10^6$ W/m² to $1,3 \cdot 10^6$ W/m² for the laminar flow regime. Regarding to the value θ_{\max} for the laminar flow regime, $\theta_{\max} = 0$ regardless of the airflow velocity u_∞ . For the turbulent flow regime, within the investigated change range $u_\infty = 7 \cdot 10^2 \dots 2 \cdot 10^3$ m/s values θ_{\max} range from $19 \dots 23^\circ$, showing minimal variation for θ_{\max} . These results are in full agreement with the experimental data.

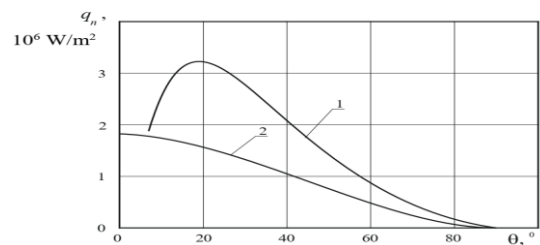


Fig. 2 – Heat flow distribution along the surface of the fairing during its supersonic blowing by air flow ($T_0 = 300$ K; $R_w = 1,5 \cdot 10^{-2}$ m; $u_\infty = 2 \cdot 10^3$ m/s): 1 – turbulent flow regime; 2 – laminar flow regime

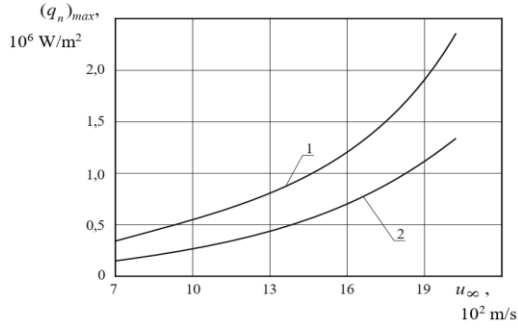


Fig. 3 – Dependence of the maximum values of the heat flow $(qn)_{max}$ on the speed of the supersonic air flow of the fairing ($T_0 = 300$ K; $R_w = 1,5 \cdot 10^{-2}$ m): 1 – turbulent flow regime; 2 – laminar flow regime

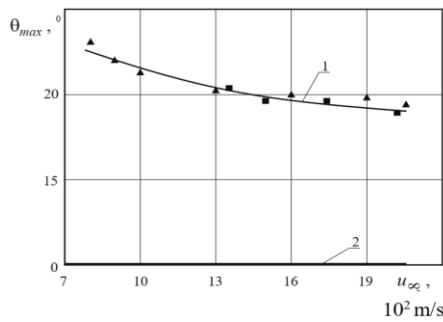


Fig. 4 – Dependence $\theta_{max}(u_\infty)$ for different supersonic flow regimes ($T_0 = 300$ K; $R_w = 1,5 \cdot 10^{-2}$ m): 1 – turbulent flow regime; 2 – laminar flow regime; $\blacktriangle, \blacksquare$ – results of experimental studies

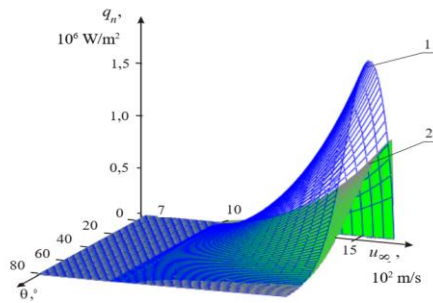


Fig. 5 – An image of the heat flow $q_n(\theta, u_\infty)$ distribution on the outer surface of the hemisphere flowing around the supersonic flow ($T_0 = 300$ K; $R_w = 1,5 \cdot 10^{-2}$ m): 1 – turbulent flow regime; 2 – laminar flow regime

Mathematical Modeling of the Thermal Impact of Supersonic Air Flow on Pyramidal Fairings.

When optical fairings of pyramidal shape are subjected to supersonic air flow, as in the case of hemispherical fairings, uneven heating of their surfaces occurs. This leads to the formation of cracks, chips, and other defects, which ultimately result in the destruction of the fairings [5, 6, 18] (Fig. 6).

The heat evaluation of the fairing will be carried out for the case of its symmetric air flow (with the angles of attack and slip being zero) (see Fig. 6).

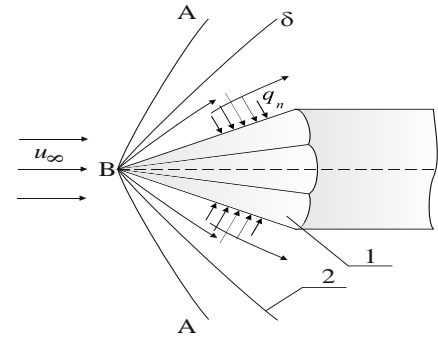


Fig. 6 – Heat map of the fairing: 1 – polyhedral pyramid; AA – shock wave front (oblique shock compression); B – front critical point (flow velocity is zero); 2 – outer boundary of the boundary layer with thickness δ ; q_n – heat flux from the boundary layer to the surface of the fairing; index “ ∞ ” – values of parameters in the incoming air flow

In this case, in the first approximation, it can be assumed that each face of the pyramid is heated equally. Therefore, we will consider the heating of the pyramid using the example of heating one of its faces, which we will approximate as a flat plate with thickness H (Fig. 7) [7, 8, 12, 17].

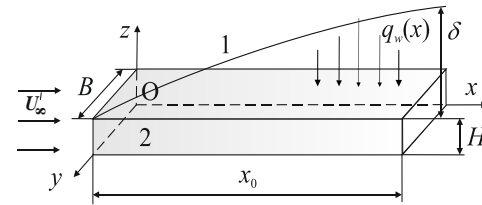


Fig. 7 – Heating scheme of the plate: 1 – external gas flow; 2 – plate; $U'_\infty = U_\infty \cdot \cos \alpha$ (α – angle of inclination of the pyramid's faces relative to the Ox axis; δ – thickness of the dynamic boundary layer; x_0, B – length and width of the plate, respectively; $q_w(x)$ – distribution of the heat flux along the plate's surface

Also, as in the case of a hemispherical fairing, using the known gas-dynamic relations [5, 6, 18], we obtain the following expression for the heat flow in the case of a turbulent flow regime:

$$q_w(x) = \frac{0,001}{Pr^{0,6}} \cdot \left(\frac{\beta \cdot x_0}{U'_\infty} \right)^{4/5} \cdot \left(\frac{v_\infty}{U'_\infty \cdot x_0} \right)^{1/5} \cdot \left(\frac{\rho_\delta}{\rho_\infty} \right)^{4/5} \times \left(\frac{\mu_\delta}{\mu_\infty} \right)^{1/5} \cdot \rho_\infty \cdot U'_\infty \cdot C_P \cdot (T_r - T_w) \cdot \left(\frac{x}{x_0} \right)^{3/5} \quad (13)$$

where $v_\infty = \mu_\infty / \rho_\infty$ - is the coefficient of kinematic viscosity of the undisturbed gas flow.

Similarly, for the laminar regime of flow around the plate (for zero angles of attack and slip), the heat flow can be given in the form

$$q_w(x) = \frac{0,05}{Pr^{0,4}} \cdot \left(\frac{\beta \cdot x_0}{U'_\infty} \right)^{1/2} \cdot \left(\frac{v_\infty}{U'_\infty \cdot x_0} \right)^{1/2} \times \left(\frac{\rho_\delta}{\rho_\infty} \right)^{1/2} \cdot \left(\frac{\mu_\delta}{\mu_\infty} \right)^{1/2} \cdot \rho_\infty \cdot U'_\infty \cdot C_P \cdot (T_r - T_w) \quad (14)$$

For further detailing of formulas (13) and (14), we will use the known gas-dynamic relations:

$$\beta = \frac{U'_\infty}{2 \cdot x_0} \cdot \left(\frac{8 \cdot (\gamma_\infty - 1) \cdot M^2 + 2}{(\gamma_\infty + 1) \cdot M^2} \times \left[1 + \frac{\gamma_\infty - 1}{2} \cdot \frac{(\gamma_\infty - 1) \cdot M^2 + 2}{2 \cdot \gamma_\infty \cdot M^2 - (\gamma_\infty - 1)} \right]^{\frac{1}{\gamma_\infty - 1}} \right)^{1/2} \quad (15)$$

where $\gamma_\infty = C_P/C_V = 1,4$ (air).

The ratios ρ_δ/ρ_∞ and μ_δ/μ_∞ are determined by calculating pressure according to Newton's method and adiabatic expansion from the critical point along the surface of the plate (in the x direction):

$$\frac{\rho_\delta}{\rho_\infty} = 6,35 \cdot \left(1 - \frac{1}{7 \cdot M^2} \right)^{-2,5} \cdot \left(1 + \frac{5}{M^2} \right)^{-1} \cdot \bar{P}^{5/2} \quad (16)$$

$$\frac{\mu_\delta}{\mu_\infty} = 0,447 \cdot M \cdot \left(1 + \frac{5}{M^2} \right)^{1/2} \cdot \frac{1 + S/T_\infty}{1 + S/T_T} \cdot \bar{P}^{3/14} \quad (17)$$

where S - is Sutherland's constant ($S = 110,4$ K); \bar{P} - the ratio of the pressure on the outer boundary of the boundary layer P_δ to the braking pressure P_T ; T_T - braking temperature.

Based on the comparison of experimental data, a fairly accurate (relative error 3...5%) formula for determining the pressure distribution in the x direction was obtained (for $M > 2...3$ and $x/x_0 < 1,2...1,5$):

$$\bar{P} = \frac{P_\delta}{P_T} = 1 - (1,525 - 1,85 \cdot k_0) \cdot \left(\frac{x}{x_0} \right)^2 + (0,487 - 1,323 \cdot k_0) \cdot \left(\frac{x}{x_0} \right)^4 \quad (18)$$

where k_0 - is the air density after a direct jump:

$$k_0 = \frac{\gamma_\infty - 1}{\gamma_\infty + 1} + \frac{2}{(\gamma_\infty + 1) \cdot M^2} \quad (19)$$

The pressure at the braking point is determined by the formula:

$$P_T = P_\infty \cdot M^2 \cdot \frac{\gamma_\infty - 1}{2} \cdot \left[\frac{(\gamma_\infty - 1) \cdot M^2}{4 \cdot \gamma_\infty \cdot M^2 - 2 \cdot (\gamma_\infty - 1)} \right]^{\frac{1}{\gamma_\infty - 1}} \quad (20)$$

The braking temperature is:

$$T_T = T_\infty \cdot \left(1 + \frac{\gamma_\infty - 1}{2} \cdot M^2 \right) \quad (21)$$

When performing calculations, the Pr_δ number for air can be considered constant at a value of 0,71, as it exhibits minimal dependence on temperature. The specific heat capacity of air C_P for the case of ideal gas flow can also be regarded as a constant value, equal to $C_P = 10^3$ J/kg·K.

Using the derived formulas (13) – (21) and standard application software packages, calculations were performed to determine the distributions of heat flux from the boundary layer along the surface of the plate under various operational conditions of the devices (Figs. 8–10).

The calculation results presented in Figs. 8–10 indicate that the location of the maximum heat flux values $(q_w)_{max}$ on the plate surface depends on the flow regime: for laminar flow, $(q_w)_{max}$ values are located near the leading critical point ($x = 0$) of the plate, whereas for turbulent flow, the $(q_w)_{max}$ shift from $x = 0$ to x_{max} . As the airflow velocity increases from $M = 2$ to $M = 6$, the heat flux values $(q_w)_{max}$ rise from $0,5 \cdot 10^5$ W/m² to $7 \cdot 10^5$ W/m² (turbulent flow) and from $0,2 \cdot 10^5$ W/m² to $3,5 \cdot 10^5$ W/m² (laminar flow). Regarding x_{max} , for laminar flow, $x_{max} \approx 0$ remains independent of M . For turbulent flow (within the investigated range of $M = 2...6$), x_{max} lies within $(0,38...0,43) \cdot x_0$ (for example, for $x_0 = 0,1$ m – $x_{max} = 0,038...0,043$ m), showing negligible variation, which fully aligns with the obtained experimental results.

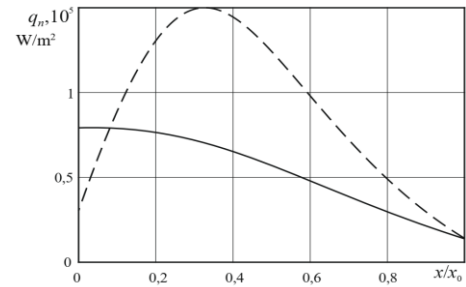


Fig. 8 – Distribution of the heat flow q_w along the surface of the plate during supersonic blowing by air flow over the object ($T_0 = 300$ K; $x_0 = 0,1$ m; $M = 3$): - - - - turbulent flow regime; — — — laminar flow regime

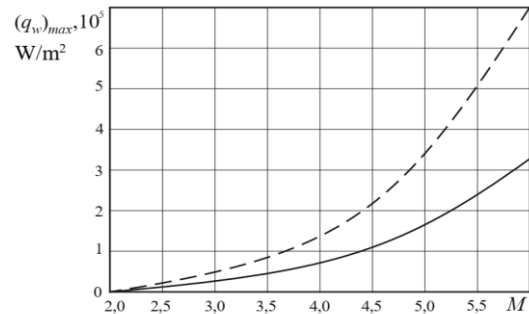


Fig. 9 – Dependence of the maximum values of the heat flow $(q_w)_{max}$ on the speed of the supersonic air flow of the plate ($T_0 = 300$ K; $x_0 = 0,1$ m): - - - - turbulent flow regime; — — — laminar flow regime

Thus, for the practical airflow velocities used for pyramid-shaped fairings ($M = 1,4...3,6$), a laminar flow regime (Reynolds criterion $Re = (L \cdot U_\infty)/\nu_\delta < 10^5$, where $U_\infty = 470,93...1201,59$ m/s, $\nu_\delta = 0,147 \cdot 10^{-4}$ m²/s for $T = 300$ K) is observed only near the leading critical point (at distances on the order of $10^{-3} ... 10^{-2}$ m).

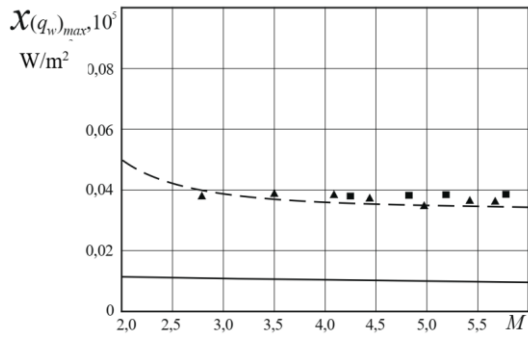


Fig. 10 – Dependence of the location on the plate surface $(q_w)_{\max}$ on the supersonic airflow velocity over the object ($T_0 = 300$ K; $x_0 = 0,1$ m): - - - - turbulent flow regime; ———— laminar flow regime; $\blacktriangle, \blacksquare$ – results of experimental studies

At greater distances, flow turbulence occurs ($Re > 10^{-5}$), leading to the emergence of additional heat generation and the formation of regions on the pyramid-shaped fairing's surfaces with maximum values of external heat flux from the boundary layer $(q_w)_{\max}$ at distances on the order of $(0,3 \dots 0,4) \cdot S$ (S - being the distance from the leading critical point of the fairing). In this case, the intensity of external thermal impacts on the fairing increases sharply, which may result in the destruction of these regions

3. CONCLUSION

1. It has been established that, for the specified ranges of flight velocities, as in the case of hemispherical fairings, a turbulent flow regime is realized over most of their surfaces, and hazardous areas emerge. By additionally treating these areas with an electron beam

(which increases the resistance of surface layers to thermal and mechanical impacts, as experimentally confirmed for hemispherical fairings and visibility windows in the form of flat plates made from optical ceramics such as KO1, KO2, KO12, etc.), their destruction during operation can be prevented.

2. It has been shown that in the case of pyramidal fairings subjected to supersonic airflow, the shock wave in the form of an oblique shock is located at the sharp leading edge, which experiences intense pressure gradients realized within the shock. In contrast, for hemispherical fairings (or fairings with a blunted leading edge, such as meniscus shapes and others), the shock wave is no longer situated on the fairing itself but at some distance from it (a so-called detached shock wave). In this case, the intensity of the pressure gradient's impact on the fairing is reduced. Therefore, during the operation of fairings with different geometric shapes at high flight speeds (above $2 \cdot 10^3 \dots 3 \cdot 10^3$ m/s), the thermal and mechanical impact (due to pressure gradients in the shock wave) is more intense for fairings with sharp leading edges (pyramids, cones, etc.), leading to their faster destruction under flight conditions.

3. It has been determined that at lower flight speeds (primarily in subsonic regimes), where a laminar flow regime is predominant over most of the fairing's surface, the intensity of thermal and mechanical effects decreases significantly (heat generation occurs only at the front critical point, and critical stresses along the surface are absent), and destruction is virtually non-existent. Therefore, in this case, it is advisable to use fairings with a sharp leading edge (pyramidal, conical, etc.), as their aerodynamic efficiency, defined by the drag coefficient C_x , is 1,5 to 2 times lower.

REFERENCES

1. *Applied Gas Dynamics, 2nd Edition* (Ed. by Ethirajan Rathakrishnan) (Wiley, John Wiley & Sons, LTD: 2019).
2. *Fundamentals of Gas Dynamics, 2nd Edition* (Ed. by V. Babu) (Springer Cham: 2021).
3. *Infrared Homing* (Ed. by Gerd Numitor) (Flu Press, 2011).
4. *Handbook of Optical Materials* (Ed. by Marvin J. Weber) (CRC Press, Boca Raton, Florida: 2003).
5. *Aerodynamics of Missiles and Rockets Hardcover* (Ed. by Mark Pinney) (McGraw-Hill Education: 2014).
6. *High Speed Flow* (Ed. by C.J. Chapman) (Cambridge University Press: 2000).
7. I.V. Yatsenko, S.V. Antonyuk, V.I. Gordienko, V.A. Vaschenko, *J. Nano- Electron. Phys.* **9** No 1, 01010 (2017).
8. I.V. Yatsenko, V.S. Antonyuk, V.I. Gordienko, O.V. Kiritchenko, V.A. Vaschenko, *J. Nano- Electron. Phys.* **10** No 4, 04028 (2018).
9. *The Mathematical Theory of Non-Uniform Gases* (Ed. by Sydney Chapman) (Cambridge University Press: 1991).
10. *Encyclopedia of Fluid Mechanics* (Ed. by Ethirajan Rathakrishnan) (Taylor & Francis: 2022).
11. I.V. Yatsenko, V.S. Antonyuk, V.A. Vashchenko, O.V. Kyrychenko, O.M. Tishchenko, *J. Nano- Electron. Phys.* **11** No 2, 02014 (2019).
12. I.V. Yatsenko, V.S. Antonyuk, V.A. Vashchenko, V.I. Gordienko, S.O. Kolinko, T.I. Butenko, *J. Nano- Electron. Phys.* **14** No 4, 04012 (2022).
13. *Heat and Mass Transfer* (Ed. by Rajendra Karva) (Springer: 2021).
14. *Fundamentals of Heat and Mass Transfer* (Ed. by T.L. Bergman) (Wiley, John Wiley & Sons, LTD: 2011).
15. *Convective Heat Transfer: Solved Problems* (Ed. by Michel Favre-Marine) (Wiley, John Wiley & Sons, LTD: 2009).
16. *Principles of Convective Heat Transfer* (Ed. by Massoud Kaviany) (Springer New York: 2013).
17. I.V. Yatsenko, V.S. Antonyuk, V.P. Maslov, V.A. Vashchenko, V.I. Gordienko, S.O. Kolinko, T.I. Butenko, *J. Nano- Electron. Phys.* **15** No 5, 05030 (2023).
18. *Computational Aerodynamics* (Ed. by Anthony Jameson) (Cambridge University Press: 2022).

Визначення ділянок на поверхні оптичних обтічників різної геометричної форми, що піддаються максимальним термоударним впливамІ.В. Яценко¹, В.С. Антонюк², В.А. Ващенко¹, В.І. Гордієнко¹, С.О. Колінько¹, Т.І. Бутенко¹,¹ *Черкаський державний технологічний університет, 18030 Черкаси, Україна*² *Національний технічний університет України «КПІ ім. Ігоря Сікорського», 03056 Київ, Україна*

Розроблені математичні моделі нагріву оптичних обтічників ГЧ-приладів різної геометричної форми (півсферичної, пірамідальної та ін.) зовнішнім надзвуковим потоком повітря. Визначені ділянки на поверхні обтічників, що піддаються максимальним термоударним впливам для різних режимів обтікання (ламінальний, турбулентний), які призводять до їх руйнувань і відмова ГЧ-приладів в умовах пострілу та польоту. Встановлені переваги і недоліки розглядуваних обтічників в залежності від швидкості їх польоту. Встановлено, що для вказаних діапазонів зміни швидкостей польоту виробів, також, як й у випадку півсферичних обтічників, на більшій частині їх поверхні реалізується турбулентний режим обтікання та виникають небезпечні ділянки, додатково оброблюючи які електронним променем (підвищується стійкість поверхневих шарів до термічних та механічних ударів) можна попереджати їх руйнування при експлуатації. Тому при експлуатації обтічників різної геометричної форми при великих швидкостях польоту (вище $2 \cdot 10^3 \dots 3 \cdot 10^3$ м/с) більш інтенсивний термічний та механічний вплив (через перепад тисків в ударній хвилі) буде для обтічників з гострою передньою кромкою (піраміда, конус та ін.), що призводить до більш швидкого їх руйнування в умовах польоту.

Ключові слова: Оптико-електронне приладобудування, Математичні моделі, Надзвуковий потік повітря, Інфрачервоні (ГЧ) прилади в умовах пострілу і польоту, Оптична кераміка, Електронно-променева технологія.